

pubs.acs.org/JPCA Article

Microwave and Computational Study of Pivalic Sulfuric Anhydride and the Pivalic Acid Monomer: Mechanistic Insights into the RCOOH + SO₃ Reaction

Nathan Love, Casey A. Carpenter, Anna K. Huff, Christopher J. Douglas, and Kenneth R. Leopold*



Cite This: J. Phys. Chem. A 2022, 126, 6194–6202



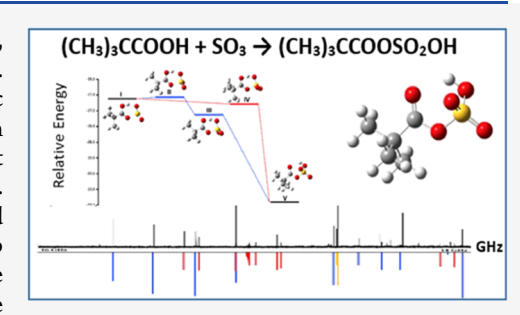
ACCESS I

Metrics & More

Article Recommendations

Supporting Information

ABSTRACT: The microwave spectrum of pivalic sulfuric anhydride, $(CH_3)_3CCOOSO_2OH$ (PivSA), has been observed by rotational spectroscopy. The compound was formed by the reaction of SO_3 with $(CH_3)_3CCOOH$ (pivalic acid) in a supersonic jet in a manner analogous to that previously observed with other carboxylic acids. Computational analysis indicates that the reaction is best described as a pericyclic process coupled with a 60° rotation of the *t*-butyl group. Product formation can occur through either a sequential (two-step) or a concerted (one-step) pathway. The former involves an internal rotation of the *t*-butyl group through a 0.11 kcal/mol barrier followed by the pericyclic reaction that joins the moieties. The latter passes through a second-order saddle point in which the internal rotation and pericyclic reaction occur simultaneously. This path is the



most energetically favorable, as the zero-point corrected energy at the saddle point structure is 0.16 kcal/mol below that of a putative (CH₃)₃CCOOH–SO₃ precursor complex. Additional computational work involving a series of carboxylic acids is reported, which explores the effects of gas-phase acidity and basicity of the RCOOH reactant on reaction energetics. These calculations, together with prior experimental and theoretical studies of the acetic and trifluoroacetic derivatives, demonstrate that the basicity of the carbonyl oxygen, not the acidity of the COOH proton, is the important driving factor for the reaction. As a precursor to the experimental work on the title molecule, microwave spectra of the parent and OD forms of the pivalic acid monomer were recorded and are reported here as well. A convenient synthesis of SO₃ is also described.

INTRODUCTION

Previous work in our laboratory has shown that carboxylic sulfuric anhydrides (CSAs) can be readily formed through a low-to-no barrier pericyclic reaction between a carboxylic acid (RCOOH) and SO_3^{1-5} viz.,

In cases where the R group of the carboxylic acid is a 3-fold rotor such as in acetic or trifluoroacetic acid (R = CH₃, CF₃), the orientation of the rotor relative to the carboxyl moiety differs between that in the complex and that in the product. Thus, reaction 1 for these species is accompanied by an additional 60° rotation of the R group. As a result, the potential energy surfaces for these systems have both a pair of transition states corresponding to the internal rotation and the pericyclic reaction, as well as a second-order saddle point corresponding to a concerted process in which the internal rotation and pericyclic reaction occur concurrently.

For most of the CSAs studied to date, the barriers to product formation relative to the putative precursor complexes are small and, in some cases, negative. For instance, the zeropoint corrected barriers for R = H, s-cis $H_2C = CH$, and HC = Care 0.26, -0.22, and 0.01 kcal/mol at the CCSD(T)/CBS(D-T)//M06-2X/6-311++G(3df,3pd) level of theory. For R = CH₃, the sequential and concerted transition state energies are 0.057 kcal/mol and -0.12 kcal/mol, respectively, at the same level of theory. In contrast, however, the zero-point corrected barriers to the formation of the trifluoroacetic acid derivative, CF₃COOSO₂OH, through either the sequential or concerted pathways are considerably higher than those of the other previously studied CSAs (1.17 and 1.21 kcal/mol, respectively). This result is consistent with our experimental observation that signal strengths for trifluoroacetic sulfuric anhydride were notably lower than those for the other anhydrides studied, though dipole moment components may also have played a role. The reason for the heightened zeropoint corrected barrier to the formation of the trifluoroacetic acid derivative is unclear but could be due to (i) the mass

Received: July 11, 2022 Revised: August 21, 2022 Published: September 6, 2022





effects associated with the 60° rotation of the relatively massive trifluoromethyl group and/or (ii) the electronic effects of the trifluoromethyl group on the activation barrier for the pericyclic reaction. A direct comparison between $R=CH_3$ and $R=CF_3$ does not address this question because the methyl group of acetic acid is both a light rotor and electron donating, while the CF_3 group in the trifluoroacetic acid is both more massive and highly electron withdrawing.

In this work, we report a computational and microwave study of pivalic sulfuric anhydride (PivSA), which was formed in a supersonic jet from pivalic acid, (CH₃)₃CCOOH, and SO₃. The reason for studying the pivalic acid reaction is that while the CF₃ and C(CH₃)₃ groups are similar in their mass distribution, they are quite different electronically, with the former being electron withdrawing and the latter being electron donating. Acetic and pivalic acids, however, are more similar in their electronic character but differ significantly in the mass of the rotor. Thus, a comparison of the reactions of SO₃ with acetic, trifluoroacetic, and pivalic acids should help to further explore the energetics of CSA formation. This goal is further supported by computations, also presented here, which explore the gas-phase acidity and basicity of a series of carboxylic acids that have been observed to react with SO₃. Microwave spectra of the parent and OD forms of the pivalic acid monomer were also obtained in preparation for this work and are reported here as well, as is a convenient laboratory preparation of SO₃.

■ COMPUTATIONAL METHODS AND RESULTS

Geometry and frequency calculations were performed at the M06-2X/6-311++G(3df,3pd) level of theory using Gaussian 6.0.16.6 Electronic energies are reported, as they directly define the potential energy surface of the system. The zero-point corrected energies are also reported because they have a significant influence on the effective activation barriers, as described below. The predicted structures and atomic numbering for the pivalic acid-SO3 complex as well as that of the anhydride product are shown in Figure 1. Calculations were also performed on the pivalic acid monomer. Atomic Cartesian coordinates for all minimum energy structures (precursor, anhydride, and monomer) are given in the Supporting Information. For all species studied, the calculated minimum energies were improved with single-point CCSD(T) calculations at the M06-2X/6-311++G(3df,3pd) geometries using the complete basis set extrapolation scheme of Neese and Valeev between the ANO-pVDZ and ANO-pVTZ basis sets (CBS(D-T)). Zero-point energy corrections were applied using M06-2X/6-311++G(3df,3pd) frequencies. These levels of theory were chosen to be consistent with our previous CSA studies. 1-5 Table 1 summarizes the important results of the calculations and includes analogous results for the acetic and trifluoroacetic acid systems for comparison. Figure 2 displays the calculated energies of the precursor complex and the anhydride product (labeled I and V, respectively) relative to that of the isolated free monomers. After zero-point corrections, the precursor complex and the anhydride lie 17.1 and 20.4 kcal/mol, respectively, lower in energy than the sum of the energies of the free monomers.

Inspection of the calculated structures reveals that the transition between the precursor complex and the anhydride involves a 60° rotation of the *t*-butyl group. Specifically, in both species, the in-plane methyl group is nearly eclipsed with the carbonyl oxygen, with torsional angles of 14 and 4° for the

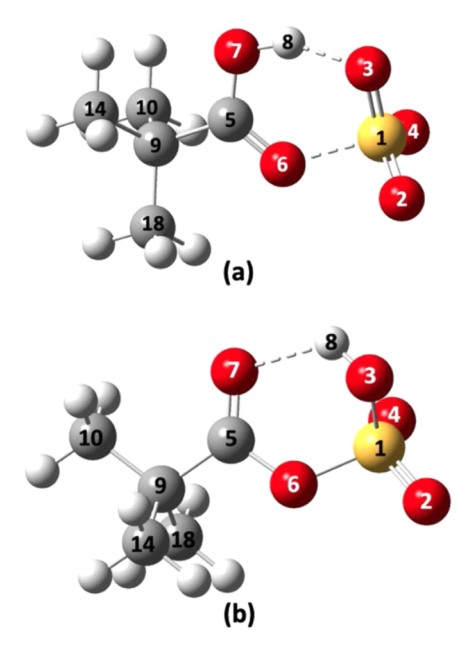


Figure 1. Predicted structures of (a) pivalic acid— SO_3 complex and (b) PivSA determined from geometry calculations at the M06-2X/6-311++G(3df,3pd) level of theory. In panel (a), the dotted lines represent the hydrogen bond and a nucleophilic association interaction. In panel (b), the dotted line represents an intramolecular hydrogen bond.

precursor complex and anhydride, respectively. However, since reaction 1 converts the OH oxygen to the C=O oxygen, the rotation must take place to maintain the near-eclipsed orientation. A similar rotation has been noted for the reactions with acetic² and trifluoroacetic acids.⁴ The 3-fold barrier to internal rotation of the t-butyl group with respect to the O7-C5-O6 plane was calculated by imposing a 60° rotation of the former and subsequently searching for a transition state at the M06-2X/6-311++G(3df,3pd) level. The result was the transition state shown as structure II in Figure 2, which, using CCSD(T) energies, lies 0.11 kcal/mol higher in energy than the minimum energy structure before zero-point corrections (0.05 kcal/mol after zero-point corrections). The 0.11 kcal/mol value is the potential barrier for internal rotation and is surprisingly lower than the corresponding value similarly determined for free pivalic acid (0.73 kcal/mol). The internal rotation barriers, V_3 , are also given in Table 1.

After the rotation of the t-butyl group, the barrier for reaching the pericyclic transition state (structure III in Figure 2) from the internal rotation transition state was determined to be 1.56 kcal/mol (1.67 kcal/mol from the minimum energy of the precursor complex). However, after zero-point corrections, the energy of structure III is 0.52 kcal/mol below that of the precursor. Thus, with zero-point energy taken into account, the only barrier to product formation is the 0.05 kcal/mol due to internal rotation of the t-butyl group. Alternatively, a secondorder saddle point (IV) was found in which the internal rotation and pericyclic reaction occur simultaneously. The barrier for this concerted pathway was calculated to be 2.08 kcal/mol above that of the precursor complex without zeropoint corrections but 0.16 kcal/mol below that of the precursor complex when zero-point corrections are applied. Thus, after zero-point corrections, there is no barrier to product formation passing through the saddle point. These results are also shown in Figure 2, in which the sequential and

Table 1. Theoretical Results for Pivalic Sulfuric Anhydride and Related Systems a

	free acid	precursor complex	anhydride
	ΔE relative to fre	ee monomers (kcal/mo	ol)
pivalic		-18.6 (-17.1)	-22.1 (-20.4)
acetic		-17.2 (-15.7)	-20.7 (-18.9)
trifluoroacetic		-11.5 (-10.2)	-16.2 (-14.4)
	V_3 ((kcal/mol) ^b	
pivalic	0.73 (0.74)	0.11 (0.05)	1.15 (1.23)
acetic	0.44 (0.36)	0.11 (0.06)	0.65^{c} (0.53)
trifluoroacetic	0.64 (0.62)	0.38 (0.35)	0.78 (0.77)
	R(S	1–O6) (Å)	
pivalic		1.903	1.621
acetic		1.932	1.626
trifluoroacetic		2.148	1.648
O	verall sequential p	athway barrier (kcal/m	ol) ^d
pivalic		1.67 (0.05) ^e	
acetic		$1.89 (0.06)^e$	
trifluoroacetic		3.29 (1.17)	
	concerted pathy	vay barrier (kcal/mol)	<i>d</i>
pivalic		2.08 (-0.16)	
acetic		2.10 (-0.12)	
trifluoroacetic		3.39 (1.21)	

^aValues determined at the CCSD(T)/CBS(D-T)//M06-2X/6-311+ +G(3df,3pd) level of theory as described in the text. Values in parentheses include zero-point corrections using M06-2X/6-311+ +G(3df,3pd) frequencies. Values for the acetic and trifluoroacetic acid derivatives are from refs 2 4, and 5. bV_3 is the potential barrier for internal rotation of the CX₃ group (X = H, F, or $\overline{CH_3}$). Experimental value is 0.68932(9) kcal/mol (reference 2). ^dThe sequential pathway for the formation of PivSA proceeds through structures II and III in Figure 2. The concerted pathway proceeds through structure IV in Figure 2, which is a second-order saddle point. Acetic and trifluoroacetic species proceed through analogous structures for both pathways. For the pivalic and acetic species, the 60° rotation transition state in the sequential pathway determines the barrier after zero-point energy corrections (rather than the pericyclic transition state, which determines the barrier without zero-point corrections). Thus, the 1.67 and 1.89 kcal/mol barriers arise from the pericyclic transition state (III) without zero-point corrections. With zero-point corrections, the barrier (0.05 or 0.06 kcal/mol) is due to internal rotation. For the trifluoroacetic species, the pericyclic transition state has the highest energy, with or without zero-point corrections, and determines the barrier in either case.

concerted pathways are highlighted in blue and red, respectively. The barriers calculated for both pathways are summarized in Table 2. Cartesian coordinates for the calculated transition state and saddle point structures are also included in the Supporting Information.

Because reaction 1 involves both the donation of a carbonyl oxygen lone pair and the transfer of the COOH proton to the SO₃, it is of interest to assess both the acidity of the proton and basicity of the oxygen to better understand the effects of the R group on the reaction energetics. The gas-phase acidities and basicities are defined in terms of the free energy changes for the following reactions, ⁸ respectively,

$$RCOOH \rightarrow RCOO^{-} + H^{+}$$
 (2)

$$RCOOH + H^+ \rightarrow RCOOH_2^+$$
 (3)

Reaction 2 provides a measure of the ease with which a proton is donated by the carboxylic acid, with smaller values corresponding to stronger acids. Reaction 3 is a rough gauge

of the basicity of the carbonyl oxygen (though it does not rigorously measure its Lewis basicity toward SO₃). The gasphase basicity is defined as the negative of the free energy change for Reaction 3, with higher values corresponding to stronger bases. The free energy of the hydrogen cation has been calculated to be -0.010012 Hartree assuming the enthalpy as 5/2RT, a temperature of 298.15 K, and using the entropy value of 108.946 J/(mol·K).9 The free energies of the neutral, protonated, and deprotonated carboxylic acids at 298.15 K were determined in Gaussian16 from frequency calculations performed at the M06-2X/6-311++G(3df,3pd) level of theory and subsequently combined with that of the hydrogen cation to determine free energy changes for reactions 2 and 3. The gas-phase acidity and basicity of other carboxylic acids observed to form CSAs are listed in Table 2 alongside their respective transition barriers to reaction with SO₃ determined from the CCSD(T) calculations. Experimental values are included for comparison where available. 10-14

■ EXPERIMENTAL METHODS AND RESULTS

Preparation of Sulfur Trioxide. SO₃ appears to be no longer commercially available, and thus, while it is a known product of the thermal decomposition of K2S2O8 or $K_2S_2O_{7}^{15,16}$ the following procedure was employed to produce the compound on a scale appropriate for the experiments performed in this work. To a 1-neck 100 mL round bottom flask equipped with a stir bar and a 14/20 short-path distilling head (thermometer joint 10/18) with a 25 mL receiving flask, was added P2O5 (183 mmol, 52.10 g) and fuming sulfuric acid (20% SO₃) (153 mmol, 15.00 g, 7.79 mL). The distilling flask was heated initially to 90 °C in an oil bath, then raised in 10 °C increments approximately every 5 min. The first collection of clear, colorless liquid was at an oil bath temperature of approximately 135 °C, with a thermometer temperature reading of approximately 45 °C. The oil bath temperature was gradually raised to 160 °C to continue collection until the thermometer temperature decreased by several degrees, and the distillation was then removed from heat. Approximately 9.40 g (117 mmol, 77% yield) of colorless, liquid sulfur trioxide were collected. A photograph of the apparatus is included in the Supporting Information.

All reagents were of reagent grade and used without further purification. Distillation was carried out using flame-dried glassware under a static nitrogen atmosphere, with lightly greased joints additionally sealed with Glindemann PTFE sealing rings. Room temperature water was used in the shortpath condenser to prevent solid SO₃ from forming and clogging the condenser. The nitrogen line was split, with one end attached to the distilling head and the other attached to a gas inlet into a sealed, 100 mL "dead flask" also equipped with an outlet line. This line was terminated with a \sim 12 gauge steel needle piercing a septum-stoppered, 500 mL round bottom flask containing ~250 mL of 6 M NaOH aqueous quench solution and equipped with a gas outlet line terminating in an oil bubbler. Prior to beginning the reaction, the distilling head gas line needle was submerged in the aqueous quench so escaping SO₃ gas bubbled through. Rubber septa and Tygon laboratory tubing were used. Warning: sulfur trioxide reacts violently with water, fumes in ambient atmosphere, degrades most materials except Teflon, and is readily carried by dynamic argon/nitrogen gas resulting in leaking of sealed joints. The freshly distilled reagent is best used immediately for desired reactions. Teflon stopcock sealed Schlenk glassware is

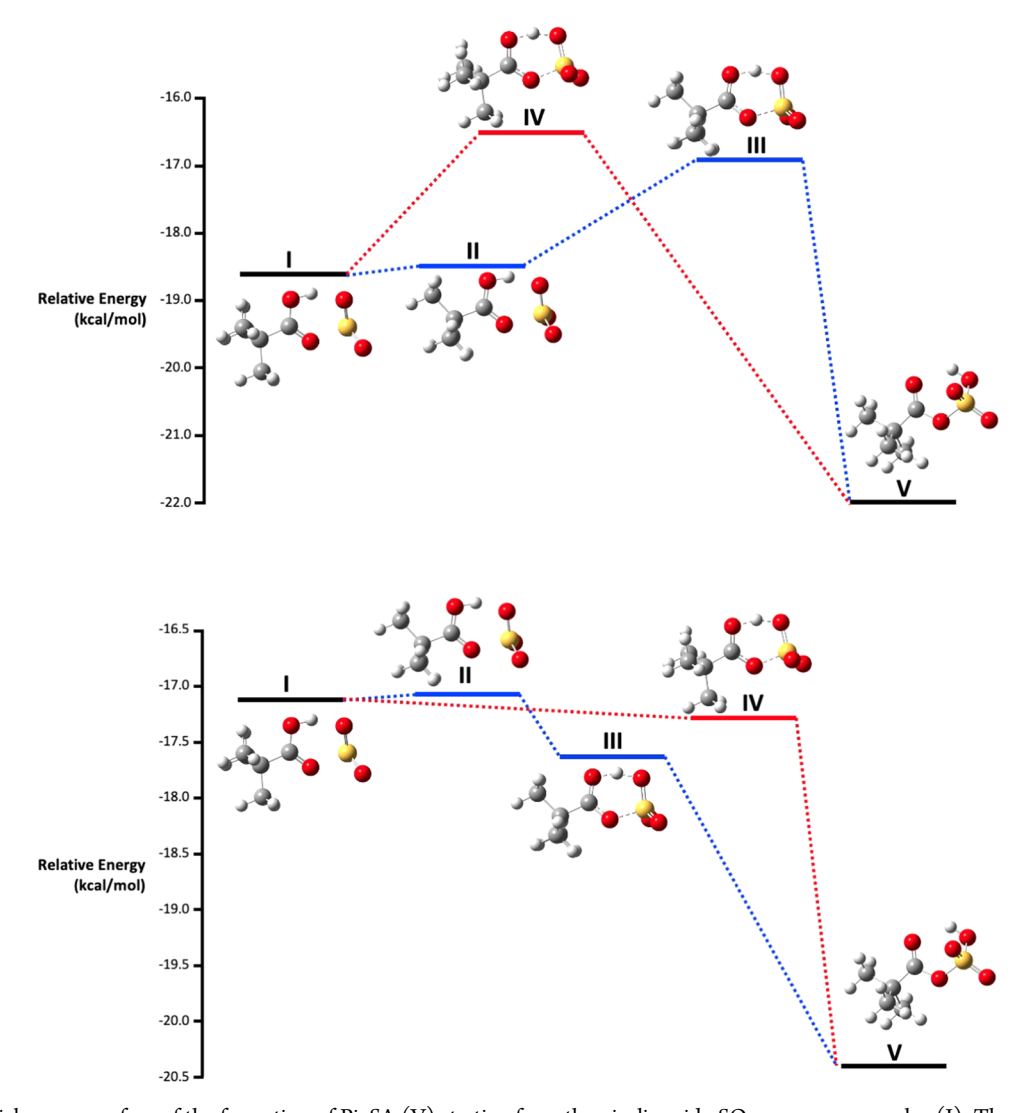


Figure 2. Potential energy surface of the formation of PivSA (V) starting from the pivalic acid— SO_3 precursor complex (I). The sequential pathway in which a 60° rotation of the *t*-butyl group precedes the pericyclic transition state is represented in blue and passes through structures II and III. The red pathway represents the concerted pathway in which structure IV is the second-order saddle point. The top figure displays CCSD(T)/CBS(D-T)//M06-2X/6-311++G(3df,3pd) electronic energies uncorrected for zero-point energy. The sequential and concerted barriers to formation are 1.56 and 2.08 kcal/mol, respectively. The bottom figure displays CCSD(T)/CBS(D-T)//M06-2X/6-311++G(3df,3pd) electronic energies corrected for zero-point energy. The sequential and concerted barriers to formation are -0.05 and -0.16 kcal/mol, respectively.

Table 2. Experimental and Theoretical Properties of CSA Precursor Carboxylic Acid Monomers

		gas-phase acidity (kcal/mol)		gas-phase basicity (kcal/mol)	
R group	barrier to CSA formation ^a (kcal/mol)	calcd ^b	exp	calcd ^b	exp
CF ₃ ^c	$1.17 (1.21)^d$	315.2	317.4(20) ^e	160.4	162.7 ^f
H^g	0.26	336.5	$339.2(15)^h$	169.9	169.8 ^f
C≡CH ⁱ	0.01	326.5		177.2	
CH_3^j	$0.057 (-0.12)^d$	339.4	341.1(20) ^f	180.4	179.9 ^f
$CH=CH_2 (s-trans)^k$	-0.22	336.0	$337.2(28)^{l}$	183.7	
$CH=CH_2 (s-cis)^k$	-0.33	336.3		184.6	
$C(CH_3)_3^m$	$0.05 \ (-0.16)^d$	336.8	338.0(20)	188.9	

^aCCSD(T)/CBS(D-T)//M06-2X/6-311++G(3df,3pd) energies with zero-point corrections from M06-2X/6-311++G(3df,3pd) frequencies. ^bTheoretical values obtained from M06-2X/6-311++G(3df,3pd) thermodynamic calculations as described in the text. ^cReference 4. ^dValue outside of parentheses corresponds to the barrier of the sequential pathway of the CF₃, C(CH₃)₃, or CH₃ transition state followed by the pericyclic transition state. Value inside the parentheses corresponds to the barrier of the simultaneous pathway in which CF₃, C(CH₃)₃, or CH₃ rotation and the pericyclic processes occur simultaneously via a second-order saddle point. Values include zero-point corrections. ^eReference 10. ^fReference 11. ^gReference 12. ^fReference 2. ^kReference 3. ^fReference 14. ^mThis work.

recommended for long-term storage of SO₃, which eventually polymerizes¹⁷ but can be liquefied by heating to 40 °C

Table 3. Spectroscopic Constants of Pivalic Acid

	(CH ₃) ₃ CCOOH			(CH ₃) ₃ CCOOD		
	obs. [MHz]	calcd [MHz]	$(obs calcd)^a [MHz]$	obs. [MHz]	calcd [MHz]	$(obs calcd)^a [MHz]$
A [MHz]	3315.00358(21)	3346.7	-31.7 (-1.0%)	3300.61293(65)	3331.4	-30.8 (-0.9%)
B [MHz]	2368.64502(18)	2393.5	-24.9 (-1.0%)	2303.71608(45)	2327.5	-23.8 (-1.0%)
C [MHz]	1991.08702(15)	2007.8	-16.7 (-0.8%)	1940.11926(44)	1955.8	-15.7 (-0.8%)
$\Delta_{\rm I}$ [kHz]	0.2306(92)			0.236(21)		
$\Delta_{\rm IK}$ [kHz]	2.3233(62)			2.139(37)		
$\Delta_{\mathrm{K}} \left[\mathrm{kHz} ight]$	-2.204(16)			-1.995(44)		
$\delta_{ m J}$ [kHz]	0.0348(10)			0.0330(71)		
$\delta_{\mathrm{K}} \left[\mathrm{kHz} \right]$	-5.8238(71)			-5.862(67)		
χ_{aa} [MHz]				0.2545(23)		
$(\chi_{\rm bb} - \chi_{\rm cc})$ [MHz]				0.0380(52)		
N^{b}	41			$23(65)^c$		
RMS [kHz]	3.9			2.6		
$ \mu_{a} \; [D]$		0.9				
$ \mu_{ m b} $ $[D]$		1.5				
$ \mu_{c} $ [D]		0.0				

[&]quot;Observed value minus that calculated at the M06-2X/6-311++G(3df,3pd) level of theory. Number in parentheses is the (obs. – calcd) expressed as a percent of the observed value. "Number of transitions in the least squares fit. "Number in parenthesis indicates the number of deuterium hyperfine components assigned."

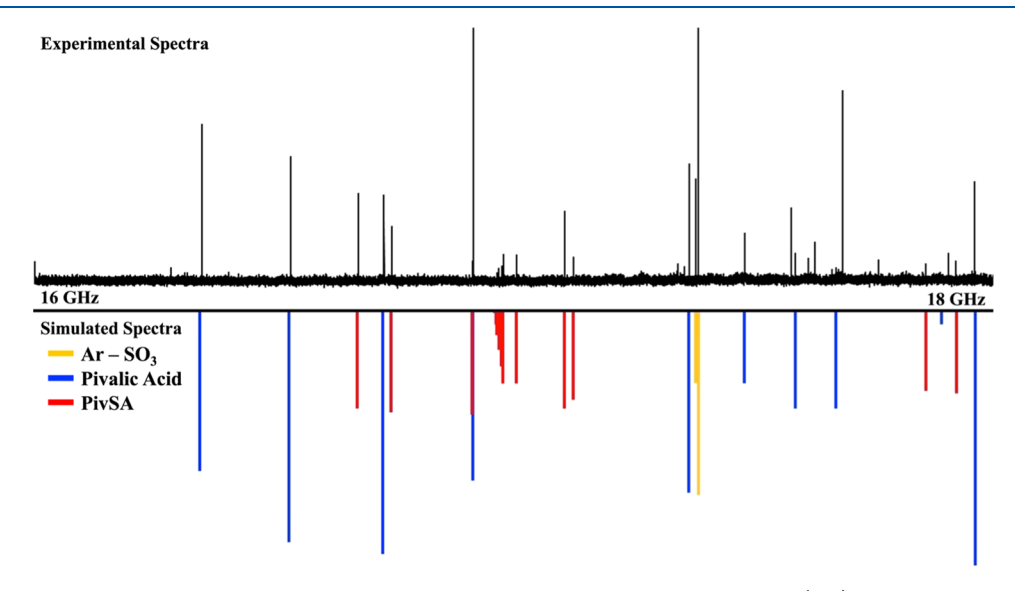


Figure 3. Microwave chirped-pulse spectrum of a pivalic acid/SO₃/Ar mixture between 16 and 18 GHz (top), and the calculated spectra of PivSA using fitted constants (bottom). Observed transitions of Ar–SO₃ are also indicated. Note that the calculated relative spectral intensities of the three species are not comparable.

overnight. Melting of solid, polymerized SO_3 can lead to pressure build-up and should be done in a hood with a blast shield.

Measurement and Assignment of Microwave Spectra of the Pivalic Acid Monomer. Spectra of the pivalic acid monomer were first measured with our tandem cavity¹⁸ and chirped-pulse¹⁹ spectrometer, details of which have been described elsewhere.^{20,21} Experimental uncertainties on measured transition frequencies are estimated to be approximately 3 kHz on the cavity system and 10 kHz on the chirped-pulse spectrometer. Pivalic acid (99% purity, purchased from Sigma-Aldrich) was introduced into the vacuum system by continuously flowing 0.6 atm of argon over a few grams of solid pivalic acid (melting point = 35 °C) to entrain its vapor in the flowing gas. The resulting pivalic acid—argon mixture was injected through a 0.016 in. hypodermic needle along the axis of a pulsed Ar expansion with a stagnation pressure of 1.0

atm. Singly deuterated pivalic acid, (CH₃)₃CCOOD, was synthesized according to a literature procedure.²² The chirpedpulse spectra were initially assigned using DAPPERS,²³ and the higher sensitivity cavity method was subsequently employed to measure lower intensity transitions for both isotopologues and resolve nuclear hyperfine splitting for OD-pivalic acid. No evidence of internal rotation was observed for either isotopologue.

Spectra were well fit using the Watson A-reduced Hamiltonian in the I^r representation ²⁴ using Pickett's SPFIT program. ²⁵ Only the quartic centrifugal distortion terms were required. For the OD species, deuterium quadrupole coupling constants were also included. Fitted spectroscopic constants are given in Table 3 and compared with calculated values. Note that the value of $\delta_{\rm K}$ is somewhat large but not egregiously so. However, a fit using the Watson S-reduced Hamiltonian made no tangible difference. Also included in the table are calculated

Table 4. Spectroscopic Constants of PivSA

	(CH ₃) ₃ CCOOSO ₂ OH	$(CH_3)_3CCOOSO_2OD$	$(CH_3)_3CCOO^{34}SO_2OH$
A [MHz]	1976.53327(37)	1950.673(25)	1976.041(29)
B [MHz]	621.914269(34)	620.35633(13)	617.273994(76)
C [MHz]	589.252788(30)	585.99770(13)	585.060380(81)
$\Delta_{ m J} [{ m kHz}]$	0.01910(18)	0.01890(40)	0.01738(49)
$\Delta_{ m JK} \ [m kHz]$	0.0741(29)	0.088(10)	0.084(14)
$\delta_{ m J}[{ m kHz}]$	0.00115(17)	[0.00115]	[0.00115]
N^a	73	48	22
RMS [kHz]	3.9	3.4	1.3

^aNumber of transitions in the least squares fit.

Table 5. Calculated Constants for the Anhydride and Precursor Complex and Comparison with Observed Values

		anhydride		precursor		
	observed	calculated ^a	$(obs calcd)^b$	calculated ^a	(obs. – calcd) ^k	
(CH ₃) ₃ CCOOSO ₂ OH						
A [MHz]	1976.53327(37)	1990.5	-14.0 (-0.7%)	2002.3	-25.8 (-1%)	
B [MHz]	621.914269(34)	625.8	-3.9 (-0.6%)	580.7	41.3 (7%)	
C [MHz]	589.252788(30)	592.8	-3.5 (-0.6%)	551.6	37.6 (6%)	
$ \mu_{\rm a} $ [D]		4.7		6.4		
$ \mu_{\rm b} $ [D]		0.5		0.7		
$ \mu_{c} $ [D]		0.8		0.1		
(CH ₃) ₃ CCOOSO ₂ OD						
$\Delta A [MHz]$	-25.86027	-27.1	1.2 (5%)	-23.8	-2.0 (-8%)	
$\Delta B \text{ [MHz]}$	-1.55794	-1.8	0.2 (13%)	-0.1	-1.5 (-94%)	
$\Delta C [MHz]$	-3.25509	-3.5	0.2 (7%)	-1.9	-1.4 (-42%)	
(CH ₃) ₃ CCOO ³⁴ SO ₂ OH						
$\Delta A [MHz]$	-0.49227	-0.4	-0.05 (-9%)	-0.1	-0.4 (-80%)	
$\Delta B \; [\mathrm{MHz}]$	-4.64027	-4.7	0.03 (0.6%)	-5.1	0.4 (9%)	
$\Delta C [MHz]$	-4.19241	-4.2	-0.01 (-0.3%)	-4. 6	0.4 (9%)	

^aTheoretical constants are from M06-2X/6-311++G(3df,3pd) calculations. ^bNumbers in parentheses are the percent error in the calculation, i.e., $100 \times (\text{obs.} - \text{calcd})/\text{lobsl}$. The absolute value is taken in the denominator so that *a* positive percent error on the isotope shifts indicates that the magnitude of the calculated shift exceeds that of the observed shift (both of which are negative).

values of the magnitudes of the dipole moment components, $\mu_{\rm a}$, $\mu_{\rm b}$, and $\mu_{\rm c}$, for the parent species. Note that there is good agreement between predicted and fitted rotational constants, as highlighted by the percent differences of 1% or less for both isotopologues. Moreover, although not explicitly shown in the table, the predicted isotope shifts of A, B, and C for the OD species were all within 1.1 MHz of the observed values. Tables of assigned transitions, as well as the residuals from the least squares fit, are included in the Supporting Information.

Measurement and Assignment of Microwave Spectra of Pivalic Sulfuric Anhydride. To observe the anhydride, SO₃ was introduced into the system by flowing 1.0 atm of argon through a stainless steel bubbler containing freshly synthesized SO₃. The resulting Ar/SO₃ mixture was pulsed into the vacuum chamber through a 0.8 mm diameter stainless steel cone nozzle. The configuration is similar to that previously described.⁵ Pivalic acid was introduced in the same manner outlined above. Upon introduction of SO₃ to the system, a new set of intense transitions was immediately observable in the chirped-pulse spectrum, a portion of which is shown in Figure 3. After accounting for known transitions of pivalic acid and Ar-SO₃, this new set of transitions was readily attributed to PivSA. The predicted rotational constants were entered into DAPPERS, and a fit comprised of only atype transitions was quickly obtained. Based on this fit, the higher sensitivity cavity spectrometer was used to observe several b- and c-type transitions. As with the pivalic acid

monomer, no evidence of internal rotation was observed. The *b*- and *c*-type spectra were significantly weaker than the *a*-type lines but generally comparable in intensity to each other. The hyperfine splitting in the (CH₃)₃CCOOD spectrum was too collapsed to resolve even with the higher resolution cavity spectrometer. The fitted parameters for the parent, deuterated, and naturally abundant ³⁴S isotopologues are shown in Table 4, and all assigned transitions are given in the Supporting Information. No spectra were observed that could be attributed to the pivalic acid—SO₃ complex (Figure 1a).

DISCUSSION

Table 5 compares the experimental rotational constants of the parent isotopologue with those calculated for both the anhydride and the precursor complex. It is seen from the table that the calculated constants for the former are in much better agreement with those for the latter, indicating that the observed species is indeed an anhydride. The table also gives the deuterium and ³⁴S isotope shifts in the rotational constants (which most easily enable the isotopic data to distinguish between species), and, again, it is seen that those for the anhydride are in better agreement with the experiment than those for the precursor complex. The computationally determined values of the magnitudes of the dipole moment components, $\mu_{\rm av}$ $\mu_{\rm b}$, and $\mu_{\rm c}$ are also included. Note that $\mu_{\rm b}$ and $\mu_{\rm c}$ are comparable in magnitude for the anhydride but differ by a factor of 7 for the complex. Thus, while the observation of c-

type transitions does not rigorously distinguish the precursor from the anhydride (since $\mu_c \neq 0$ in both cases), the similar intensity of the observed b- and c-type spectra would be expected for the anhydride but not the precursor. Indeed, since the observed b-type transitions were themselves rather weak, the 0.1 D value of $|\mu_c|$ of the complex would not be expected to give rise to observable spectra at all. Thus, the observation of c-type spectra and their comparable intensities to those of the b-type lines further support the conclusion that the anhydride is the species that was observed.

The S1-O6 bond in the precursor complex has a calculated bond length of 1.903 Å (Table 1). This is somewhat longer than the S-O(H) single bond in H_2SO_4 , 1.574(10) Å, ²⁷ but considerably shorter than the 2.432(3) Å intermolecular sulfur-oxygen bond in SO₃···OH₂.²⁸ Thus, as we have noted for other carboxylic sulfuric anhydrides,5 the precursor complex is best described as containing a partially formed dative bond of the kind that has been discussed at great length previously.^{29,30} Moreover, the -18.6 kcal/mol binding energy of the precursor complex is larger than that of a typical van der Waals interaction but indeed comparable to that of a partially formed dative bond. In contrast, the S1-O6 bond length in the anhydride, 1.621 Å, is almost identical to the S-O(H) bond in sulfuric acid, indicating that it is an "ordinary" covalent single bond. Correspondingly, the -22.1 kcal/mol binding energy reflects further advancement of the sulfur-oxygen partial bond in the precursor complex upon anhydride formation. The significant variation in the internal rotation barrier of the t-butyl group may, in part, reflect changes in electronic structure that accompany the progression from separated monomers to partially bound complex to a bona fide chemically bonded molecule.

As noted above and diagrammed in Figure 2, the energy barrier starting from the precursor complex is 1.67 kcal/mol for the sequential pathway. This arises from a small (0.11 kcal/ mol) internal rotation barrier of the t-butyl group followed by an additional 1.56 kcal/mol needed to reach the pericyclic transition state. However, with zero-point energy corrections, the energy of the pericyclic transition state falls below that of the precursor complex. This indicates that the only barrier to the sequential process is the small energy associated with the internal rotation. For the concerted pathway, the second-order saddle point lies 2.08 kcal/mol higher in energy than the precursor complex without zero-point corrections but is brought to 0.16 kcal/mol lower in energy when zero-point corrections are applied. Thus, passing through the saddle point (which incorporates the internal rotation) has no barrier after zero-point corrections and thus represents the most energetically favorable pathway to the product.

It is of interest to compare these results with those for the trifluoroacetic sulfuric anhydride, which as noted in the Introduction section was considerably more difficult to observe than either the pivalic or acetic derivatives. Table 1, which also includes analogous results for the acetic acid reaction, shows that, in contrast to the pivalic acid reaction, both the sequential and concerted processes for trifluoroacetic acid have positive barriers whether or not zero-point energy corrections are included. Indeed, it is seen that, of the three systems, the trifluoroacetic acid reaction is the only one for which the pericyclic transition state represents the activation barrier, even after zero-point corrections. It is interesting to note that the moment of inertia of the CF_3 group about its pseudo- C_3 axis (88 amu·Å²) is similar to that of the t-butyl group in PivSA

(111 amu·Å²). However, the internal rotation barrier in the precursor complex is somewhat larger for trifluoroacetic acid (0.38 kcal/mol vs 0.11 kcal/mol for pivalic acid). Since it is not necessarily clear whether these differences play a significant role in the difference between their respective reactions with SO₃, a simple comparison of pivalic and trifluoracetic acids is inconclusive. However, as also seen in Table 1, the barriers for both the sequential and concerted pathways in the acetic acid reaction, for which the moment of inertia of the rotor is only ~ 3 amu·Å², are very similar to those of the pivalic acid reaction, even after zero-point energy is taken into account. Since methyl and t-butyl groups are both electron releasing while the trifluoromethyl group is electron withdrawing, this suggests that the electronic character of the R group influences the overall barriers to product formation and that the requisite internal rotation plays less of a role. Zero-point energy is a crucial factor insofar as it significantly lowers the activation barriers (Table 1) and has a much more significant effect on the pericyclic transition states than it does on the internal rotation barriers. In light of these observations, the remaining focus of the discussion will be on the impact of the electronic properties of the R group of carboxylic acid on the reaction energetics.

Although, in previous work, we have loosely described reaction 1 as a cycloaddition, it more closely resembles a pericyclic hetero-ene reaction, as there is a net gain of one sigma bond and a net loss of one pi bond. Such an identification allows for further depth of understanding of the reaction mechanism. Figure 4 depicts the rearrangement of

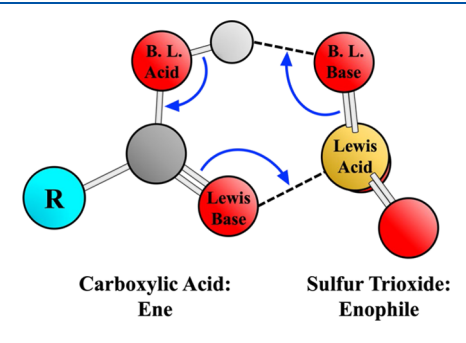


Figure 4. Structure of a generalized hetero-ene transition state between a carboxylic acid as the ene and SO₃ as the enophile. The blue arrows highlight the movement of electrons that occurs in the hetero-ene transition state. As a part of the hetero-ene reaction, the carboxylic acid behaves simultaneously as a Brønsted–Lowry acid and Lewis base. Accordingly, the hydroxyl oxygen which acts as the Brønsted–Lowry acid is labeled "B.L. Acid" and the sulfur oxygen which acts as the Brønsted–Lowry base is labeled "B.L. Base". The sulfur atom is labeled as "Lewis Acid", and the carbonyl oxygen is labeled as "Lewis Base".

electrons and bonds that occurs when the reaction takes place for any carboxylic acid (i.e., any R group). It can be seen from the figure that the carboxylic acid simultaneously behaves as both a Brønsted–Lowry acid by donating a proton to SO_3 oxygen and a Lewis base by donating electrons to the electrophilic SO_3 sulfur. In general, electron-withdrawing R groups are expected to increase the relative Brønsted–Lowry acidity and decrease the relative Lewis basicity of carboxylic acids, while electron-donating R groups have the opposite effects. Thus, electronic effects related to R set up a competition between factors that influence the energetics of the hetero-ene transition state.

The calculated acidities and basicities in Table 2 provide rough quantitative measures that help elucidate the relative importance of these two conflicting effects. From the table, it is seen that the barrier to CSA formation is largest when the gasphase acidity value of the carboxylic acid is smallest (i.e., the acid is strongest). In other words, stronger Brønsted-Lowry acids, such as trifluoroacetic acid, do not necessarily correspond to lower activation barriers. This trend would indicate that the ability of a carboxylic acid to behave as a proton donor is relatively unimportant to the hetero-ene transition state. In contrast, the CSA formation barrier appears to decrease as the gas-phase basicity of the carboxylic acid increases. These results suggest, therefore, that the hetero-ene reaction to form a CSA is driven primarily by the ability of a carboxylic acid to donate a lone electron pair to the sulfur. The energies of the anhydride products relative to those of the free monomers follow the same trend, with the magnitude of ΔE in Table 1 ordered such that $R = CF_3 < CH_3 < C(CH_3)_3$.

CONCLUSIONS

Microwave spectra of the pivalic acid monomer and its reaction product with SO₃ (pivalic sulfuric anhydride, PivSA) have been measured and assigned. Sequential and concerted reaction pathways involving a 60° rotation of the carboxylic R group and a hetero-ene transition state were determined computationally for the formation of PivSA from the pivalic acid-SO₃ precursor complex. Pivalic acid was specifically chosen for this study due to the similar mass distribution and dissimilar electronic effects of its t-butyl R group compared with those of a trifluoromethyl group. A comparison between PivSA and its acetic and trifluoroacetic acid analogs shows that the 60° rotation of the t-butyl or CF₃ group that accompanies product formation minimally impacts the reaction energetics, whereas the electronic effects related to the carboxylic R group drive the barrier height and the overall energy change for the reaction. The impact of electronic effects on the hetero-ene transition state has been further examined through the use of gas-phase acidity and basicity calculations, which show the reaction is more favorable for carboxylic acids that are weaker Brønsted-Lowry acids and stronger Lewis bases. In other words, the basicity of the carbonyl oxygen is more important than the acidity of the COOH group. Additionally, a convenient medium-to-large scale synthesis of SO₃ has been documented, as the compound has become more difficult to obtain commercially.

ASSOCIATED CONTENT

Supporting Information

The Supporting Information is available free of charge at https://pubs.acs.org/doi/10.1021/acs.jpca.2c04904.

Tables of observed and calculated frequencies for pivalic acid and pivalic sulfuric anhydride; calculated Cartesian coordinates for pivalic acid, pivalic sulfuric anhydride, and associated transition states and saddle points; and photograph of the apparatus used to synthesize SO₃ (PDF)

AUTHOR INFORMATION

Corresponding Author

Kenneth R. Leopold – Department of Chemistry, University of Minnesota, Minneapolis, Minnesota 55455, United States;

orcid.org/0000-0003-0800-5458; Email: kleopold@umn.edu

Authors

Nathan Love — Department of Chemistry, University of Minnesota, Minneapolis, Minnesota 55455, United States Casey A. Carpenter — Department of Chemistry, University of Minnesota, Minneapolis, Minnesota 55455, United States;

orcid.org/0000-0002-2539-788X

Anna K. Huff — Department of Chemistry, University of Minnesota, Minneapolis, Minnesota 55455, United States Christopher J. Douglas — Department of Chemistry, University of Minnesota, Minneapolis, Minnesota 55455, United States; Orcid.org/0000-0002-1904-6135

Complete contact information is available at: https://pubs.acs.org/10.1021/acs.jpca.2c04904

Notes

The authors declare no competing financial interest.

ACKNOWLEDGMENTS

This work was supported by the National Science Foundation (Grant No. CHE 1953528) and the Minnesota Supercomputing Institute.

REFERENCES

- (1) Mackenzie, R. B.; Dewberry, C. T.; Leopold, K. R. Gas Phase Observation and Microwave Spectroscopic Characterization of Formic Sulfuric Anhydride. *Science* **2015**, *349*, 58–61.
- (2) Huff, A. K.; Mackenzie, R. B.; Smith, C. J.; Leopold, K. R. Facile Formation of Acetic Sulfuric Anhydride: Microwave Spectrum, Internal Rotation, and Theoretical Calculations. *J. Phys. Chem. A* **2017**, *121*, 5659–5664.
- (3) Smith, C. J.; Huff, A. K.; Mackenzie, R. B.; Leopold, K. R. Observation of Two Conformers of Acrylic Sulfuric Anhydride by Microwave Spectroscopy. *J. Phys. Chem. A* **2017**, *121*, 9074–9080.
- (4) Huff, A. K.; Mackenzie, R. B.; Smith, C. J.; Leopold, K. R. A Perfluorinated Carboxylic Sulfuric Anhydride: Microwave and Computational Studies of CF₃COOSO₂OH. *J. Phys. Chem. A* **2019**, 123, 2237–2243.
- (5) Smith, C. J.; Huff, A. K.; Ward, R. M.; Leopold, K. R. Carboxylic Sulfuric Anhydrides. J. Phys. Chem. A 2020, 124, 601–612.
- (6) Frisch, M. J.; Trucks, G. W.; Schlegel, H. B.; Scuseria, G. E.; Robb, M. A.; Cheeseman, J. R.; Scalmani, G.; Barone, V.; Petersson, G. A.; Nakatsuji, H.; et al. *Gaussian 16*, revision C.01; Gaussian, Inc.: Wallingford, CT, 2016.
- (7) Neese, F.; Valeev, E. F. Revisiting the Atomic Natural Orbital Approach for Basis Sets: Robust Systematic Basis Sets for Explicitly Correlated and Conventional Correlated *Ab Initio* Methods. *J. Chem. Theory Comput.* **2011**, *7*, 33–43.
- (8) Lias, S. J.; Bartmess, J. Gas-Phase Ion Thermochemistry, in NIST Chemistry WebBook, NIST Standard Reference Database Number 69, Linstrom, P. J.; Mallard, W. G., Eds.; National Institute of Standards and Technology: Gaithersburg, MD, 20899, 2005.
- (9) Chase, M. W., Jr. NIST-JANAF Thermochemical Tables. J. Phys. Chem. Ref. Data 1998, 1–1951.
- (10) Caldwell, G.; Renneboog, R.; Kebarle, P. Gas Phase Acidities of Aliphatic Carboxylic Acids, Based on Measurements of Proton Transfer Equilibria. *Can. J. Chem.* **1989**, *67*, *611*–*618*.
- (11) Hunter, E. P. L.; Lias, S. G. Evaluated Gas Phase Basicities and Proton Affinities of Molecules: An Update. *J. Phys. Chem. Ref. Data* 1998, 27, 413–656.
- (12) Kim, E. H.; Bradforth, S. E.; Arnold, D. W.; Metz, R. B.; Neumark, D. M. Study of HCO₂ and DCO₂ by Negative Ion Photoelectron Spectroscopy. *J. Chem. Phys.* **1995**, *103*, 7801–7814.

- (13) Jinfeng, C.; Topsom, R. D.; Headley, A. D.; Koppel, I.; Mishima, M.; Taft, R. W.; Veji, S. Acidities of Substituted Acetic Acids. *J. Mol. Struct.* **1988**, *168*, 141–146.
- (14) Graul, S. T.; Schnute, M. E.; Squires, R. R. Gas Phase Acidities of Carboxylic Acids and Alcohols from Collision-Induced Dissociation of Dimer Cluster Ions. *Int. J. Mass Spectrom. Ion Processes* **1990**, 96, 181–198. (Conformer not specified).
- (15) De Vries, K. J.; Gellings, P. J. The Thermal Decomposition of Potassium and Sodium-Pyrosulfate. *J. Inorg. Nucl. Chem.* **1969**, 31, 1307–1313.
- (16) Barboott, M. M.; Jasim, F. On the Thermal Decomposition of Alkali Persulfates by Derivatograph. *Thermochim. Acta* **1976**, *16*, 402–406.
- (17) Greenwood, N. N.; Earnshaw, A. Chemistry of the Elements; Pergamon Press: Oxford, 1984.
- (18) Balle, T. J.; Flygare, W. H. Fabry-Perot Cavity Pulsed Fourier Transform Microwave Spectrometer with a Pulsed Nozzle Particle Source. *Rev. Sci. Instrum.* **1981**, *52*, 33–45.
- (19) Brown, G. G.; Dian, B. C.; Douglass, K. O.; Geyer, S. M.; Shipman, S. T.; Pate, B. H. A Broadband Fourier Transform Microwave Spectrometer Based on Chirped Pulse Excitation. *Rev. Sci. Instrum.* **2008**, *79*, No. 053103.
- (20) Phillips, J. A.; Canagaratna, M.; Goodfriend, H.; Grushow, A.; Almlöf, J.; Leopold, K. R. Microwave and Ab Initio Investigation of HF-BF₃. *J. Am. Chem. Soc.* **1995**, *117*, 12549–12556.
- (21) Dewberry, C. T.; Mackenzie, R. B.; Green, S.; Leopold, K. R. 3D-Printed Slit Nozzles for Fourier Transform Microwave Spectroscopy. *Rev. Sci. Instrum.* **2015**, *86*, No. 065107.
- (22) Ji, P.; Zhang, Y.; Dong, Y.; Huang, H.; Wei, Y.; Wang, W. Synthesis of Enantioenriched α Deuterated α Amino Acids Enabled by an Organophotocatalytic Radical Approach. *Org. Lett.* **2020**, 22, 1557–1562.
- (23) Love, N.; Huff, A. K.; Leopold, K. R. A New Program for the Assignment and Fitting of Dense Rotational Spectra Based on Spectral Progressions: Application to the Microwave Spectrum of Pivalic Anhydride. *J. Mol. Spectrosc.* **2020**, *370*, No. 111294.
- (24) Watson, J. K. G. Aspects of Quartic and Sextic Centrifugal Effects on Rotational Energy Levels, in Vibrational Spectra and Structure, Durig, J. R., Ed.; Elsevier Scientific Publishing: Amsterdam, 1977; pp 1–89.
- (25) Pickett, H. M. The Fitting and Prediction of Vibration-Rotation Spectra with Spin Interactions. *J. Mol. Spectrosc.* **1991**, *148*, 371–377.
- (26) Bowen, K. H.; Leopold, K. R.; Chance, K. V.; Klemperer, W. Weakly Bound Complexes of Sulfur Trioxide: The Structure of ArSO₃ and the Dipole Moment of N₂SO₃. *J. Chem. Phys.* **1980**, 73, 137–141.
- (27) Kuczkowski, R. L.; Suenram, R. D.; Lovas, F. J. Microwave Spectrum, Structure, and Dipole Moment of Sulfuric Acid. *J. Am. Chem. Soc.* **1981**, *103*, 2561–2566.
- (28) Phillips, J. A.; Canagaratna, M.; Goodfriend, H.; Leopold, K. R. Microwave Detection of a Key Intermediate in the Formation of Atmospheric Sulfuric Acid: The Structure of H₂O–SO₃. *J. Phys. Chem. A* **1995**, *99*, 501–504.
- (29) Leopold, K. R.; Canagaratna, M.; Phillips, J. A. Partially Bonded Molecules from the Solid State to the Stratosphere. *Acc. Chem. Res.* **1997**, *30*, 57–64.
- (30) Leopold, K. R. Partially Bonded Molecules and Their Transition to the Crystalline State. In *Advances in Molecular Structure Research*, Hargittai, M.; Hargittai, I., Eds.; JAI Press: Greenwich, CT, 1996; Vol. 2, pp 103–127.
- (31) Hoffmann, H. M. R. The Ene Reaction. Angew. Chem., Int. Ed. 1969, 8, 556–577.

☐ Recommended by ACS

Unusual Diradical Intermediates in Ozonolysis of Alkenes: A Combined Theoretical and Synchrotron Radiation Photoionization Mass Spectrometric Study on Ozonolysis...

Hanlin Fan, Liming Wang, et al.

OCTOBER 19, 2022

THE JOURNAL OF PHYSICAL CHEMISTRY A

READ 🗹

Multi-state and Multi-mode Vibronic Coupling Effects in the Photoionization Spectroscopy of Acetaldehyde

Vadala Jhansi Rani, S. Mahapatra, et al.

SEPTEMBER 20, 2022

THE JOURNAL OF PHYSICAL CHEMISTRY A

READ 🗹

M←NCCH₃, M-η²-(NC)-CH₃, and CN-M-CH₃ Prepared by Reactions of Ce, Sm, Eu, and Lu Atoms with Acetonitrile: Matrix Infrared Spectra and Theoretical Calculations

Fei Cong, Lester Andrews, et al.

NOVEMBER 08, 2021

INORGANIC CHEMISTRY

READ 🗹

Gas-Phase Formation of Fulvenallene (C_7H_6) via the Jahn-Teller Distorted Tropyl (C_7H_7) Radical Intermediate under Single-Collision Conditions

Chao He, Ralf I. Kaiser, et al.

JANUARY 21, 2020

JOURNAL OF THE AMERICAN CHEMICAL SOCIETY

READ 🗹

Get More Suggestions >